# High Surface Area of Polyhedral Chromia and Hexagonal Chromium Sulfide by the Thermolysis of Cyclohexylammonium Hexaisothiocyanatochromate(III) Sesquihydrate

Abdulaziz A. Bagabas,*[a] Murad Alsawalha,[b] Kamal K. Taha,[c] Abdelhamid Albaid,[d] Manzar Sohail,[e] Mahdi Alqahtani,[a] Rasheed Alrasheed,[a] Abdulaziz Alqarn,[a] Bandar Ashamari,[a] and Ivan P. Parkin[f]

A new organic-inorganic hybrid salt of cyclohexylammonium hexaisothiocyanatochromate(III) sesquihydrate, $(C_6H_{11}NH_3)_3[Cr(NCS)_6] \cdot 3/2H_2O$, was synthesized at room-temperature by metathesis and ligand addition for the establishment of energy-saving chemical synthesis approach. The formation of this new salt was confirmed by FT-IR, UV-Vis spectrophotometry, elemental microanalysis, and single-crystal X-ray diffraction. The TGA study showed low-temperature thermal stability of this salt, where chromium oxide ($Cr_2O_3$) formed under air and chromium sulfide ($Cr_2S_3$) under argon, as PXRD confirmed their formation as nanocrystalline. The morphological studies by SEM and TEM revealed the formation of irregular polyhedron particles of $Cr_2O_3$ and of hexagonal packed layers of $Cr_2S_3$. The textural study by nitrogen physisorption disclosed the meso-porous nature and high specific surface area of $Cr_2O_3$ (~ 132 $m^2 g^{-1}$) and $Cr_2S_3$ (~ 241 $m^2 g^{-1}$). Cyclohexylammonium could act as an organic self-template for the formation of mesopores and the high temperature of thermolysis assisted the formation of such pores.

## 1. Introduction

In recent years, the synthesis and characterization of cyclohexylammonium-based compounds are of considerable inter-est in the field of materials chemistry. The interest is primarily in the structural arrangement and its diverse dimensional properties with varying counter anions.[1–20] The attraction of using of cyclohexylammonium is specifically due to its function as a hydrogen donor for hydrogen bonding with the counter anion[1–20] and with the solvent crystallization molecules.[2,6] Furthermore, both the modelling and synthesis of novel solid-state materials by utilizing transition metal anionic complexes are a promising approach for the formation of one, two, or three-dimensional (1-D, 2-D, or 3-D) hydrogen-bonded assemblies of molecules to realize the effective functioning of the materials.[1,4,7,8,11,13,16,18–20]

Thiocyanate metal complexes are unusual due to the intrinsic ambidentate nature, bridging ability, and denticity of thiocyanate ligand.[21] Among the thiocyanate metal complexes is the anionic complex of hexaisothiocyanatochromate(III) $[Cr(NCS)_6]^{3-}$, which was used broadly to construct various supramolecular structures with either organic cations[22–30] or metal cations,[31–49] partially, because both of thiocyanate nitrogen and sulfur terminals are hydrogen acceptors when forming hydrogen bonds.[14,20,25,27–29,31–37,39–46]

[a] *Prof. A. A. Bagabas, Dr. M. Alqahtani, R. Alrasheed, A. Alqarn, B. Ashamari* National Petrochemical Technology Center (NPTC), Materials Science Research Institute (MSRI), King Abdulaziz City for Science and Technology (KACST), P O Box 6086, Riyadh 11442, Saudi Arabia
E-mail: abagabas@hotmail com
[b] *Dr. M. Alsawalha* Department of Chemical & Process Engineering Technology, Industrial Chemistry Major, Jubail Industrial College, Jubail Industrial City, P O Box 10099, 31961, Saudi Arabia
[c] *Dr. K. K. Taha* Department of Chemistry & Industrial Chemistry, College of Applied & Industrial Sciences, University of Bahri, Khartoum, Sudan
[d] *Dr. A. Albaid* Department of Physics, Faculty of Science, University of Ha'il, P O Box 2440, Ha'il 81451, Saudi Arabia
[e] *Dr. M. Sohail* Department of Chemistry, School of Natural Sciences, National University of Science and Technology, H-12, Islamabad, 44000, Pakistan
[f] *Prof. I. P. Parkin* Department of Chemistry, University College London, 20 Gordon Street, London WC1H 0AJ, United Kingdom

The organic salts of $[Cr(NCS)_6]^3$ are soluble in many organic solvents, enabling their use as analytical reagents, synthetic blocks for new compounds, catalysts, and thermally sensitive materials.[25,28,29] In addition, the incorporation of organic cation would affect both the properties of $[Cr(NCS)_6]^3$ and of the entire resultant salt.[25] For instance, when the paramagnetic anion of $[Cr(NCS)_6]^3$ was combined with charge-transfer organic π-donors of tetrathiafulvalene derivatives, the resultant salts were paramagnetic semiconductors due to their layered structures, which were composed of isolated organic cations and inorganic anions without contacts except the weak S···S contacts between cation and anion, and thereby, lack of magnetic exchange interactions.[24,26,27,30]

The metal salts of $[Cr(NCS)_6]^3$ are classified as bimetallic complexes or double complex salts.[31–49] They are able to form molecular magnets.[32] They are useful precursors for the synthesis of various functional materials, polymetallic systems, catalysts, nanocomposites, and reversible thermochromic materials.[31–49] The $[Cr(NCS)_6]^3$ , as an inert bulky ion, is a precipitating agent for lanthanide ions in organic-aqueous medium.[34–36,39,41,42,44,46–49] In addition, $[Cr(NCS)_6]^3$ is a very good reagent for the gravimetric analysis of heavy metal ions, such as copper, silver, cadmium, mercury, lead, thallium, and bismuth, in the aqueous medium, even in the microscale range.[50–56]

**Table 2.** Comparison of the scattering angles of the main peaks for experimental and simulated PXRD patterns Errors in 2V is given by $j\partial 2V_{CAL} \quad 2V_{EXP}\flat \times 100=2V_{EXP}j$

| Peak | $2V_{EXP}$ (degree) | $2V_{CAL}$ (degree) | Error in 2V % | Miller Index (h k l) |
|---|---|---|---|---|
| 1 | 6 45 | 7 26 | 12 48 | 1 0 1 |
| 2 | 9 42 | 9 54 | 1 25 | 2 1 0 |
| 3 | 10 78 | 10 97 | 1 82 | 1 0 2 |
| 4 | 14 32 | 14 55 | 1 64 | 2 0 2 |
| 5 | 15 16 | 15 35 | 1 29 | 3 1 1 |
| 6 | 17 22 | 17 44 | 1 25 | 3 1 2 |
| 7 | 18 93 | 19 15 | 1 14 | 4 2 0 |
| 8 | 20 25 | 20 50 | 1 26 | 4 1 1 |
| 9 | 21 82 | 22 11 | 1 35 | 4 1 2 |
| 10 | 23 67 | 24 06 | 1 66 | 3 1 4 |
| 11 | 24 83 | 24 50 | 1 34 | 1 0 5 |
| 12 | 25 22 | 26 01 | 3 11 | 5 3 2 |
| 13 | 28 60 | 28 90 | 1 03 | 6 3 0 |
| 15 | 28 93 | 29 25 | 1 08 | 5 1 3 |
| 16 | 31 08 | 31 39 | 1 01 | 6 1 1 |
| 17 | 32 00 | 32 36 | 1 10 | 6 3 3 |
| 18 | 36 19 | 36 64 | 1 25 | 6 1 4 |
| 19 | 38 84 | 38 73 | 0 30 | 5 1 6 |
| 20 | 57 53 | 58 30 | 1 33 | 10 0 2 |

**Table 1.** Elemental Analysis for $(C_6H_{11}NH_3)_3[Cr(NCS)_6] \cdot 3/2H_2O$

| Element | Theoretical (wt/wt %) | Experimental (wt/wt %) |
|---|---|---|
| C | 39 59 | 39 74 |
| H | 6 23 | 6 30 |
| N | 17 31 | 16 98 |
| S | 26 43 | 25 72 |
| O | 3 30 | 3 19 |
| C r | 7 14 | 6 97 |

The thermolysis, under air, of double complex salts of lanthanides, complexed by the neutral ε-caprolactam, and $[Cr(NCS)_6]^3$ results in a mixture of the corresponding lantha-nide oxide ($Ln_2O_3$) and chromia ($Cr_2O_3$) nanoparticles due to their relatively low temperatures of decomposition.[38] On the other hand, the thermolysis of heavy metal complexes with $[Cr(NCS)_6]^3$ , under air, gives metal-containing products, de-pending on the identity of the heavy metal. It results in a mixture of metal sulfate and chromia, when the heavy metal is

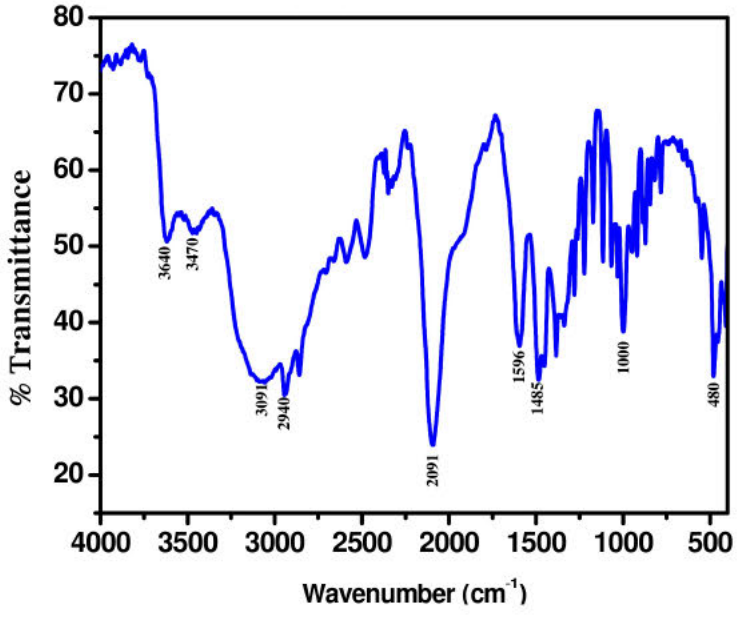


**Figure 1.** FTIR spectrum of $(C_6H_{11}NH_3)_3[Cr(NCS)_6] \cdot 3/2H_2O$

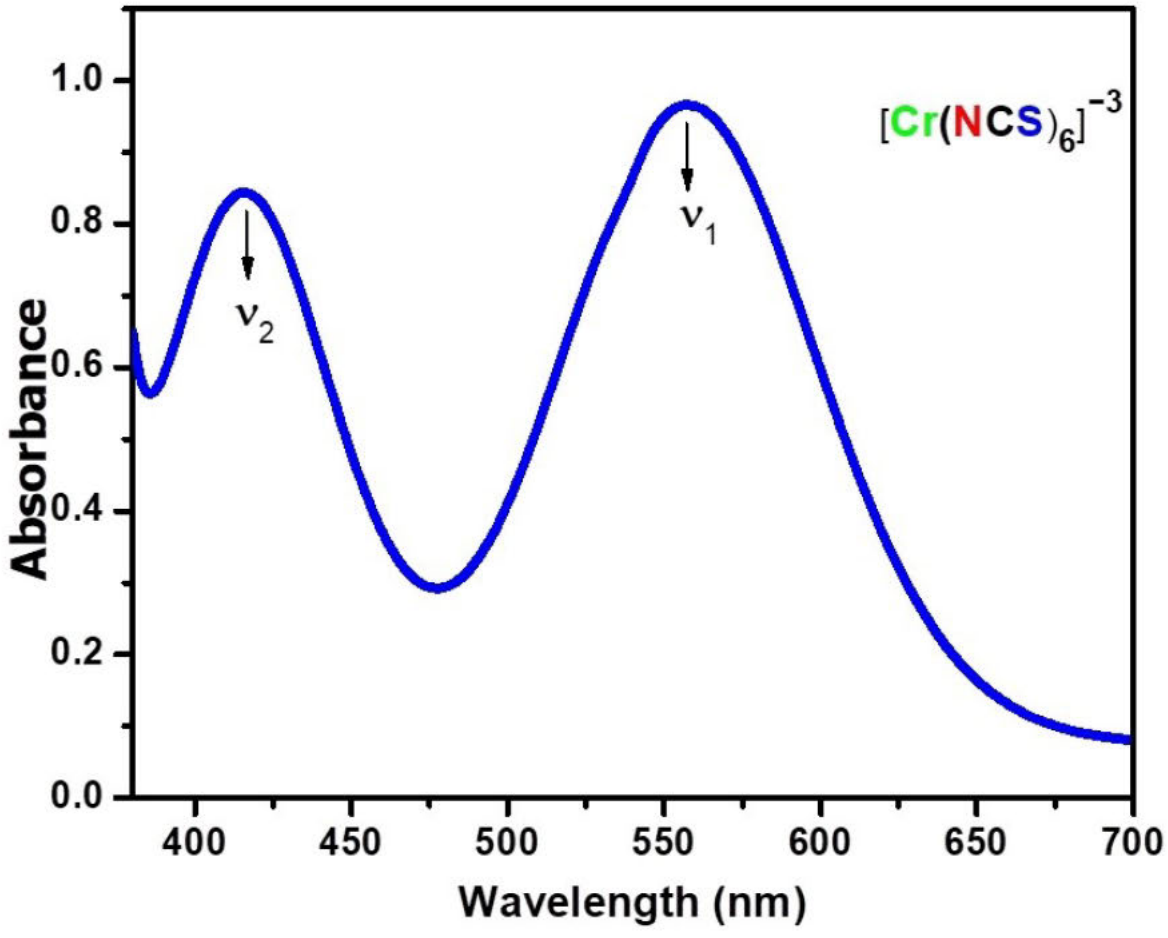


**Figure 2.** UV-Visible absorbance spectrum of $(C_6H_{11}NH_3)_3[Cr(NCS)_6] \cdot 3/2H_2O$ dissolved in EtOH

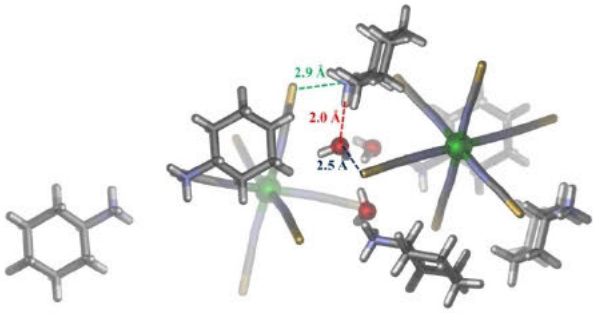


**Figure 3.** Crystal structure, showing bonding; sulfur disorder was removed for clarity

silver, thallium, lead, or bismuth,[54,55] whereas cupric oxide and delafossite ($CuCrO_2$) result when the heavy metal is cuprous and cadmium oxide and cadmium chromite spinel ($CdCr_2O_4$) result when the heavy metal is cadmium.[56]

In contrast, the thermolysis of organic salts of $[Cr(NCS)_6]^3$ has been less explored than the metal salts. In one study by House and Marquardt,[57] the thermolysis of piperidinium salt of $[Cr(NCS)_6]^3$ under nitrogen, resulted in chromium sulfide ($Cr_2S_3$), as the final chromium-containing solid product.

In the light of the importance of cyclohexylammonium and $[Cr(NCS)_6]^3$ , we report, herein, for the first time, the synthesis and the characterization of the organic-inorganic hybrid salt of cyclohexylammonium hexaisothiocyanatochromate(III) sesquihydrate, $(C_6H11NH_3)_3[Cr(NCS)_6] \cdot 3/2H_2O$, as well as its thermolysis as a single-source precursor for the synthesis of high surface area polyhedron of $Cr_2O_3$ under air and hexagonal plates of $Cr_2S_3$ under helium atmosphere. The applications of $Cr_2O_3$ are varied in number and it is especially useful as catalyst, anode for lithium-ion batteries, hydrogen absorption, gas sensor, magnetic materials, pigments, and the production of paint products.[58–68] On the other hand, the industrial applica-tions of $Cr_2S_3$ have been realized in the manufacture of catalysts, supercapacitors, and energy storage devices.[69–73]

## 2. Results and Discussion

### 2.1. Elemental analysis

Table 1 presents the elemental micro-analysis of $(C_6H_{11}NH_3)_3[Cr(NCS)_6] \cdot 3/2H_2O$. Based on the elemental results, the correlation

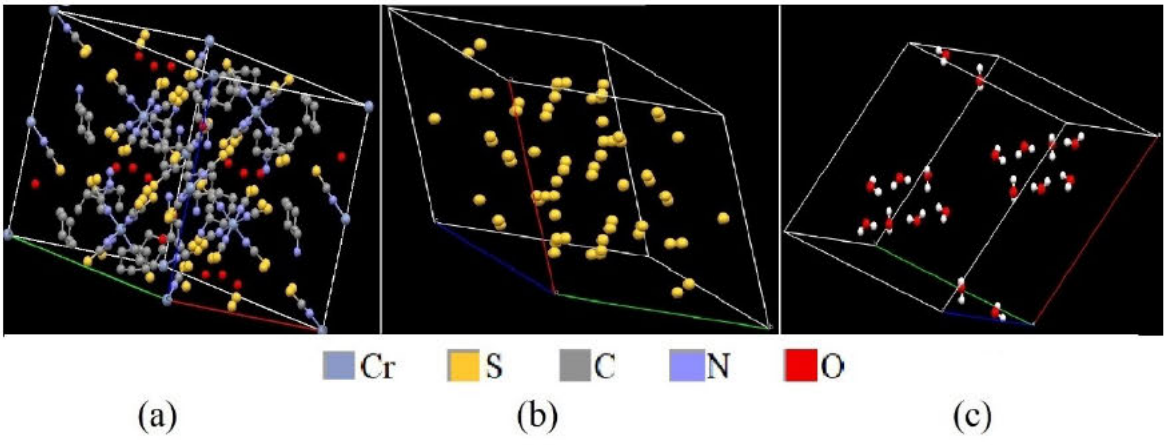


**Figure 4.** Atomic distribution inside the primitive cell obtained from Mercury for all atoms except hydrogen atoms along with their color-code (a), sulfur atoms (b), and water molecules only, where white color code refers to hydrogen atom (c)

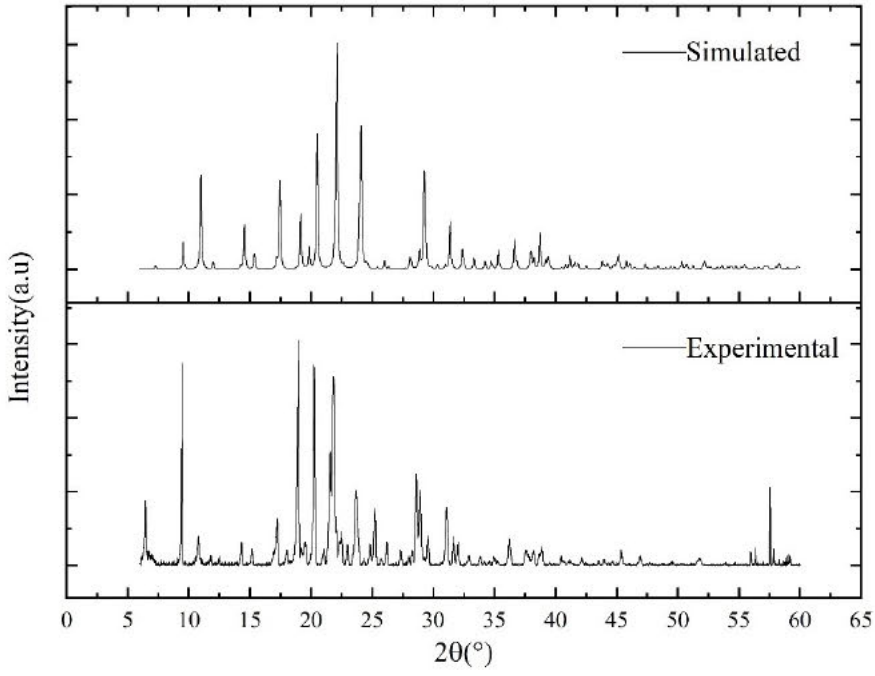


**Figure 5.** X-ray powder diffraction patterns: top is the simulated and bottom is the experimental for $(C_6H_{11}NH_3)_3[Cr(NCS)_6] \cdot 3/2H_2O$

between the theoretical and experimental results was within the acceptable error range, confirming the molecular formula of $C_{24}H_{45}N_9S_6O_{1.5}Cr$ for our synthesized hybrid organic-inorganic salt.

### 2.2. FTIR spectrophotometry

Figure 1 illustrates the DRIFT spectrum of $(C_6H_{11}NH_3)_3[Cr(NCS)_6] \cdot 3/2H_2O$. The weak, broad bands in the range of 3700–3350 cm $^{1}$ could be assigned to the asymmetric vibration of O H bonds of the crystallization water molecules.[79] The broadness of these peaks could be due to the involvement of the crystallization water molecules into intermolecular hydrogen bonds with the terminal sulfurs of $[Cr(NCS)_6]^3$ anion and with the amine protons of the cyclohexylammonium cations.[80] In addition, the band around 1600 cm $^{1}$ could be assigned to the bending mode of $H_2O$.[81] The FTIR spectrum showed characteristic vibrations of binding thiocyanate ligand via its N-terminal to the Cr(III) ion center. The main C N asymmetric stretching vibration, ν(CN), appeared as very strong band at 2091 cm $^{1}$, while the C S stretching, ν(CS), was detected as a weak band at 846 cm $^{1}$. The bending vibration of the N C S band, δ(NCS), was observed as a strong band at 480 cm $^{1}$.[32,33,35,37–39,41–49,57,85–88] The coordination of hard Cr(III) ion center by the hard N-terminal of thiocyanate ligand is consistent with Pearson's concept of hard and soft acids and

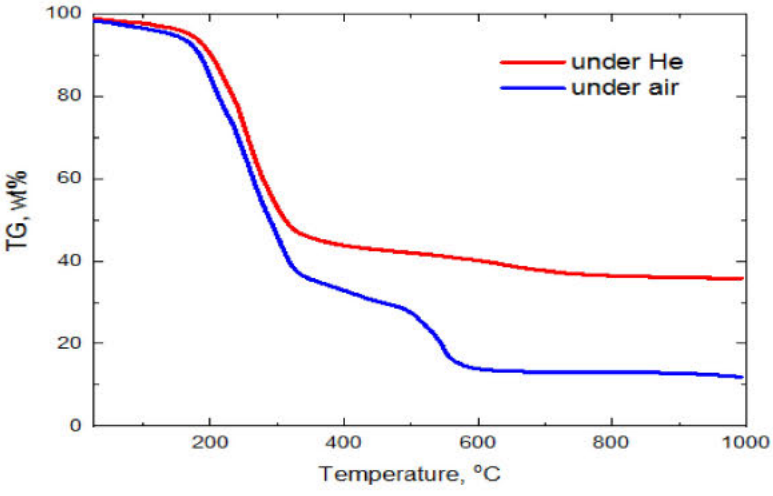


**Figure 6.** Thermogravimetric analysis of $(C_6H_{11}NH_3)_3[Cr(NCS)_6] \cdot 2H_2O$ under air (blue) and helium (red)

bases (HSAB).[34,44,57,85,86] Furthermore, structural studies by single X-ray diffraction confirmed the binding of N-terminal to Cr(III) in $[Cr(NCS)_6]^3$ .[21,24–37,39–49]

The asymmetric stretching vibration of ( $NH^+_3$) bonds of cyclohexylammonium cation could be assigned to the strong, broad bands in the range of 3300–3000 cm $^1$. This red shift in the asymmetric stretching of N H could be due to the positive charge borne by the nitrogen atom and the hydrogen bonding to the water crystallization molecules and to the S-terminals of $[Cr(NCS)_6]^3$ anion. The medium intense band at 1596 cm $^1$ could be due to N H scissoring, while the two weak bands at 1318 and 1281 cm $^1$ could be ascribed to N H wagging. The medium intense band at 920 cm $^1$ could be owing to N H twisting. The bands at 2940 and 2861 cm $^1$ could be assigned to the asymmetric and symmetric stretching vibrations of ( $CH_2$), respectively. The two medium intense bands at 1485 and 1452 cm $^1$ could be due to ( $CH_2$) deformation. The medium intense band at 1223 cm $^1$ could be owing to ( $CH_2$) wagging. The medium intense band at 1116 cm $^1$ and the weak band at 1066 cm $^1$ might be ascribed to ( $CH_2$) twisting, while the ( $CH_2$) rocking might be observed at 846 (medium), 784 (weak), 603 (very weak), 564 (weak), and 548 (weak) cm $^1$. The weak band at 1033 cm $^1$ and the strong band at 1000 cm $^1$ could be assigned to the C N stretching. The medium intense band at 874 cm $^1$ could be due to C H bending. Ring deformation could be assigned to the bands at 1172 (weak), 889 (weak), and 782 (weak) cm $^1$, while ring breathing could be ascribed to the band at 949 (medium) cm $^1$. The ring C N bending could be due to the two strong bands at 482 and 459 cm $^1$.[20,87] On the basis of FTIR analysis, the formation of $(C_6H_{11}NH_3)_3[Cr(NCS)_6] \cdot 3/2H_2O$ can be confirmed. Figure S1, in the supplementary information, shows all the FTIR bands labeled with their corresponding wavenumbers, as per the above elucidation.

### 2.3. UV-Vis spectrophotometry

The absorbance spectrum in the ultraviolet-visible region of dissolved $(C_6H_{11}NH_3)_3[Cr(NCS)_6] \cdot 3/2H_2O$ in absolute ethanol is presented in Figure 2. The two strong broad bands, with their maxima absorbance at 557 nm ($\nu_1$) and 416 nm ($\nu_2$), are characteristic for the purple, octahedral hexaisothiocyanato-chromate(III) anionic complex, $[Cr(NCS)_6]^3$ . The $\nu_1$ band refers to $^4A_{2g}(F)!^4T_{2g}(F)$ transition and the $\nu_2$ band corresponds to $^4A_{2g}(F)!$ $^4T_{1g}(F)$ transition.[22,23,32,82,83,85,88,89] The UV-visible and FTIR absorbance spectra confirmed the binding of the thiocyanate ligand via its N-terminal to the Cr(III) ion centre.

### 2.4. SXRD and PXRD

Single crystal X-ray study showed that the complex crystallized in trigonal space group *R*. The asymmetric unit consisted of two one-sixth units of hexaisothiocyanatochromate(III) anions, a cyclohexylammonium cation, and a half molecule of water due to presence of three fold axis of rotation and an inversion center. The Cr(III) ions were located on 3-fold roto-inversion axis, whereas the cyclohexylammonium cation and water molecule were situated at general positions. Each chromium ion center formed an octahedron by coordinating with six nitrogen atoms of six isothiocyanate ligands. Cyclohexylammo-nium cation adopted nearly chair confirmation, where ammonium occupies an equatorial position, as reported previously.[1–14,16–20] The oxygen-bound hydrogen atoms in water molecules were also refined by using the riding model because the X-ray data was not of sufficient quality to locate them in difference Fourier map. The sulfur atoms of isothiocyanate ligands in both complex units had disorder, which wasmod-elled over two positions in each case. The hydrogen bonding (between oxygen of water molecules and hydrogen of ammonium of cyclohexylammonium cation), chalcogen bond-ing (S···O and S···N as shown in Figure 3), and non-classical hydrogen bondings appeared to direct the packing of mole-

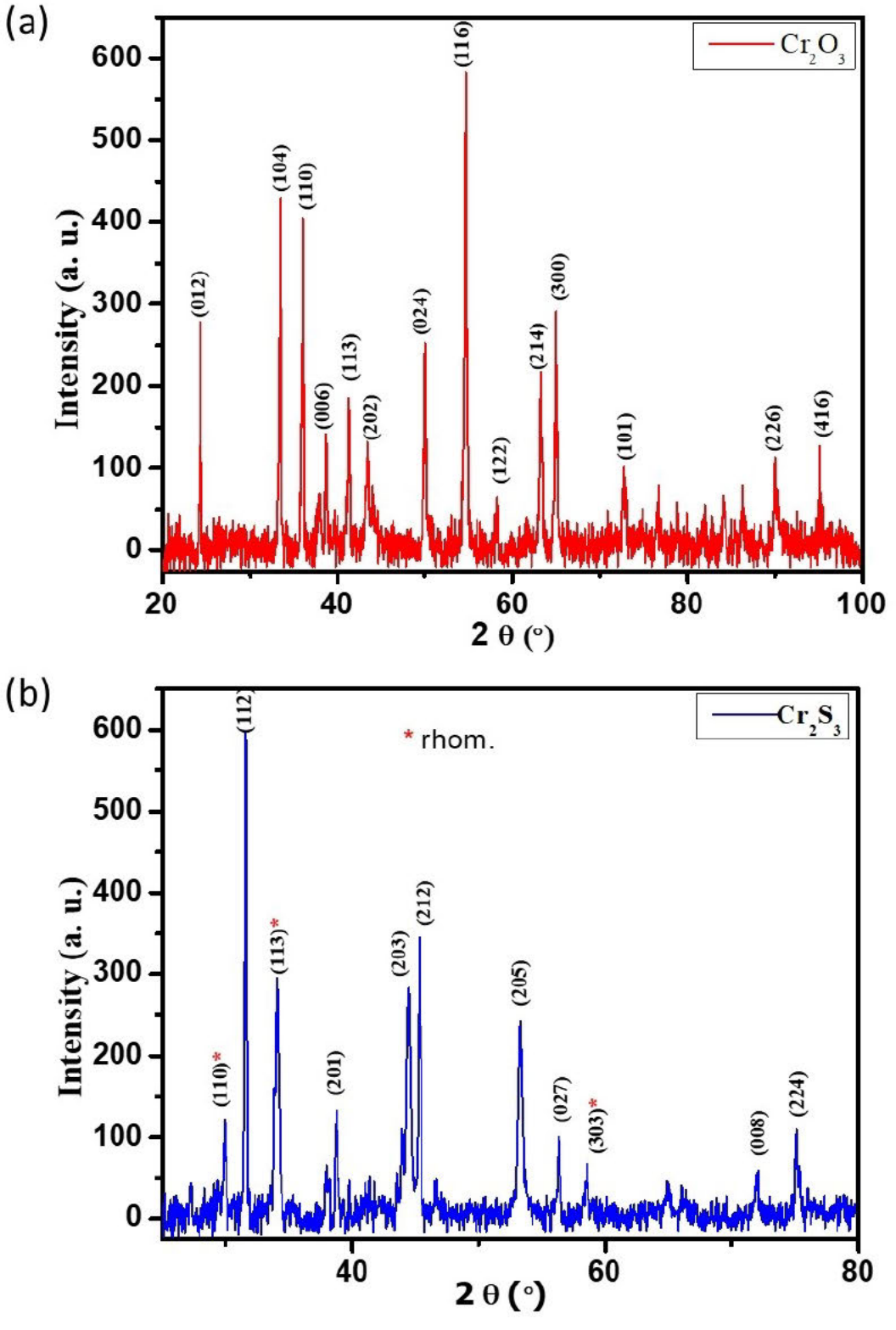


**Figure 7.** PXRD of (a) $Cr_2O_3$ and (b) $Cr_2S_3$ produced by the thermal decomposition of $(C_6H_{11}NH_3)_3[Cr(NCS)_6] \cdot 3/2H_2O$ under air and helium, respectively

cules in the lattice. These crystal features confirmed the FTIR and UV-visible spectroscopic findings.

**Crystal Data** for $C_{48}H_{90}Cr_2N_{18}O_3S_{12}$ ($M$ = 1456.07 g/mol): trigonal, space group *R3; char*=0x00*AFnotimplemented*(no. 148), $a$ = 18.5286(6) Å, $c$ = 18.6362(11) Å, $V$ = 5540.8(5) Å$^3$, $Z$ = 3, $T$ = 100(2) K, μ(MoK$_\alpha$) = 0.682 mm $^{1}$, $D_{calc}$ = 1.309 g cm $^{3}$, 14292 reflections measured (5.056 $\leq 2\Theta \leq$ 56.564 ), 3051 unique ($R_{int}$ = 0.0433, $R_{sigma}$ = 0.0292) which were used in all calcula-

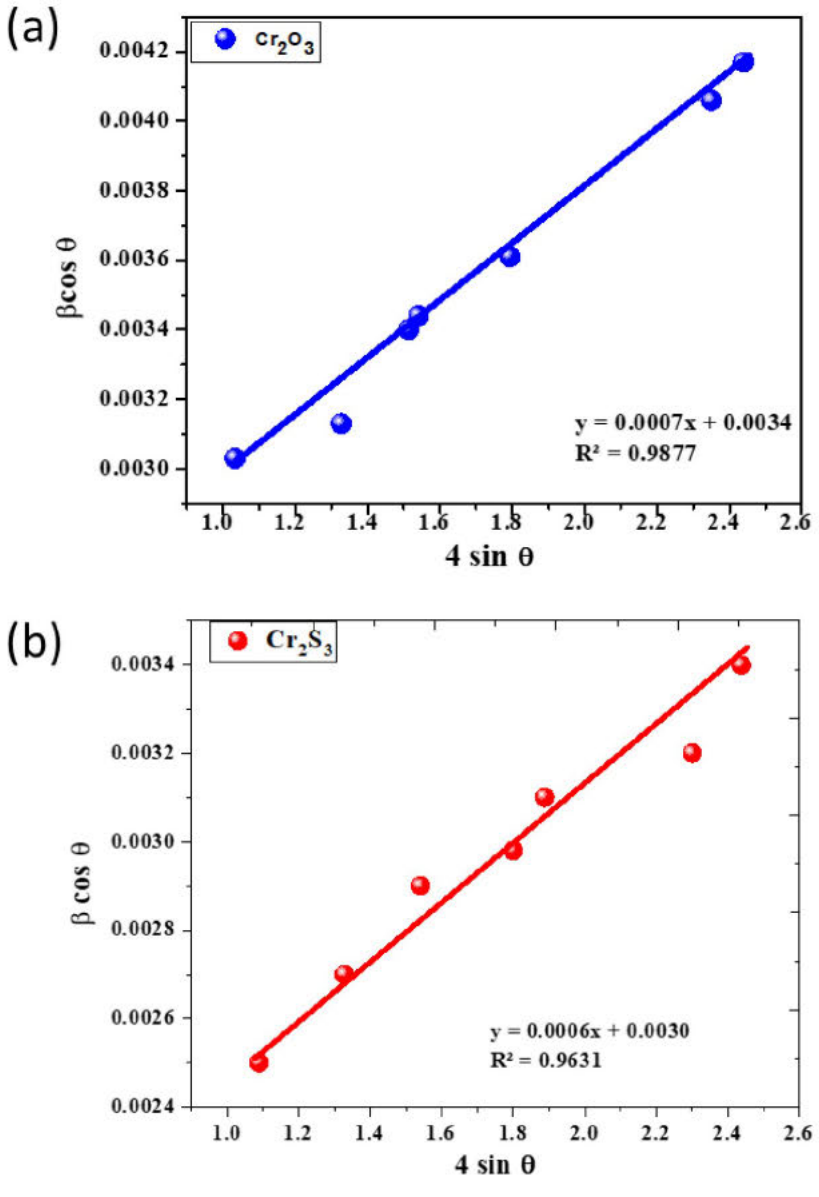


**Figure 8.** Williamson-Hall plots for (a) $Cr_2O_3$ and (b) $Cr_2S_3$ nanocrystals

tions. The final $R_1$ was 0.0738 ($I > 2\sigma(I)$) and $wR_2$ was 0.2244 (all data).

The crystal data, atomic coordinates and equivalent isotropic displacement parameters, bond lengths and angles, and anisotropic displacement parameters are given in the Tables of the supplementary information (Tables S1–S4). The bond lengths and angles of cyclohexylammonium were close to those reported in literature.[1–14,16,18–20] In addition, the bond lengths and angles of hexaisothiocyanatochromate(III) were similar to those published previously.[24–49]

The structure of $(C_6H_{11}NH_3)_3[Cr(NCS)_6] \cdot 3/2H_2O$, obtained from the X-ray diffraction of its single crystal at 100 K, is shown in Figure 4. The PXRD pattern, in the two theta range of 5.0–65.0, of the synthesized $(C_6H_{11}NH_3)_3[Cr(NCS)_6] \cdot 3/2H_2O$, con-firmed its high degree of crystallinity.[90] The structure belongs to the trigonal crystal and rhombohedral lattice system. The hexagonal unit cell for the rhombohedral Bravais lattice consists of three lattice points. The simulated PXRD pattern, based on the above structure, was generated by "Mercury" program.

The experimental PXRD pattern was compared with the simulated one, as depicted in Figure 5. This comparison was made in order to use the simulated PXRD pattern as a reference standard. We can find good match between the predicted crystal structure of the simulated pattern and the structure of the experimental pattern.[20]

The positions of main peaks for both patterns are almost matched, as illustrated in Table 2. The specimen displacement error[91] might be responsible for the small peak shifts between the simulated and experimental PXRD patterns. On the other hand, there are some peaks in the experimental PXRD pattern,

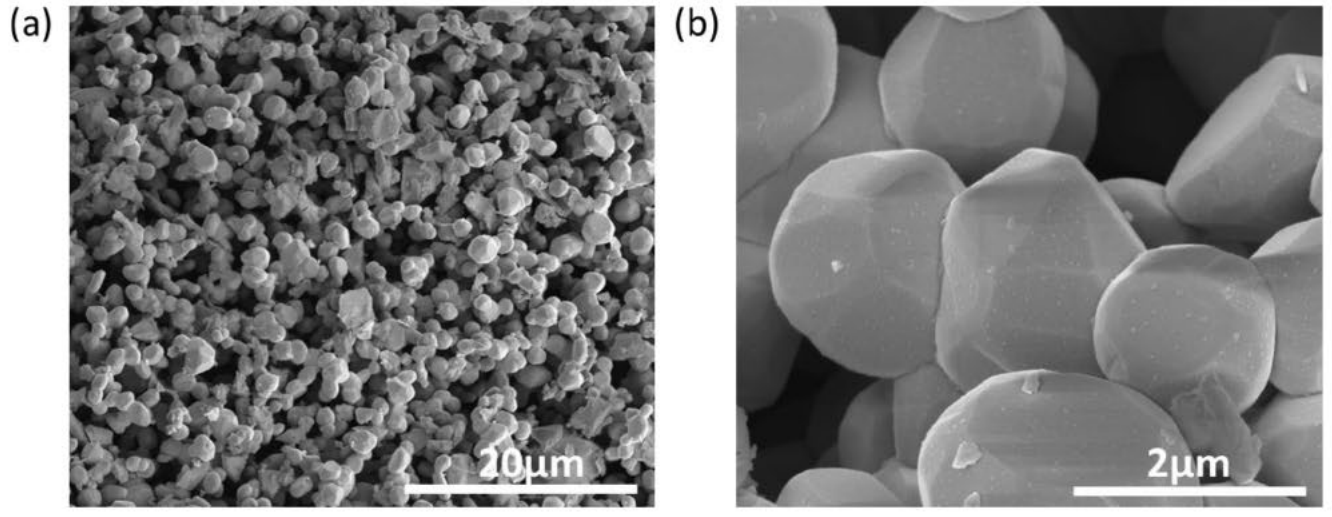


**Figure 9.** SEM electron micrograph images of $Cr_2O_3$ at magnifications of (a) × 5,000 and (b) × 50,000

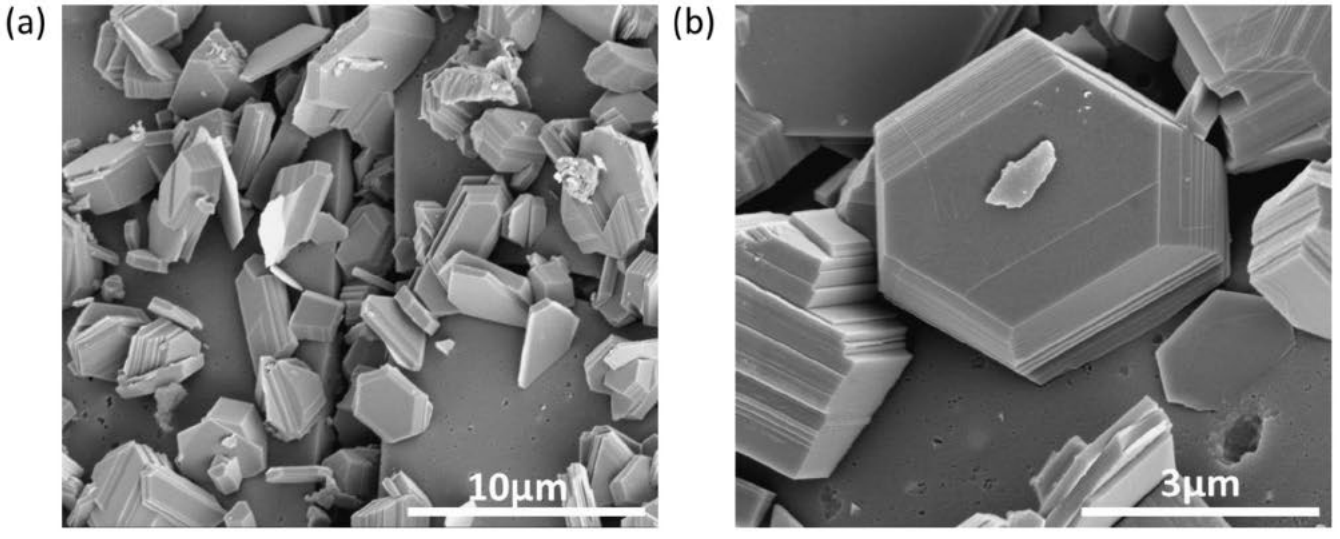


**Figure 10.** SEM micrograph images of $Cr_2S_3$ at magnifications of (a) × 10,000, (b) × 35,000

which cannot be found in the simulated pattern due to the disorders in the atomic configuration at room temperature.

The disorders in the atomic configuration can also be seen from the structure obtained by the X-ray diffraction of single crystal at 100 K. The standard number of atoms inside each cell is three multiples of the chemical formula $(C_6H_{14}N)_6(C_6CrN_6S_6)_2 \cdot 3(H_2O)$ because there are three lattice points for each cell. We found disorders in the water crystallization molecules and sulfur atoms. There were 62 sulfur atoms and 18 water molecules inside each cell instead of 36 sulfur atoms and 9 water molecules of the standard numbers, as shown in Figures 4 (b) and (c), respectively. Twenty six couples out of 62 of sulfur atoms existed at the peripheral of the anionic complex of $[Cr(NCS)_6]^3$ . This disorder in atomic configuration would be expected to increase at room temperature at which the PXRD experiment was conducted. In addition, the disorders would increase because the size occupied by water molecules at room temperature is smaller than that at 100 K. The effect of disorders on the experimental PXRD pattern can be understood through the intensity of each peak which is determined by $I_{hkl} / |F_{hkl}|$, where $F_{hkl}$ is the structural factor that determines the configuration of atoms inside crystal cell as $F_{hkl} = \sum_j f_j \exp[2\pi i(hx_j + ky_j + lz_j)]$. $f_j$ is the atomic form factor and $x_j$ , $y_j$ *and* $z_j$ are the fractional coordinates relative to the cell axes. On the other hand, one can match the positions of the main peaks of the experimental and the simulated patterns. Table 2 compares the main peak positions of the experimental and calculated powder patterns and provides their corresponding Miller indices. The overall error is around 2.0 %.

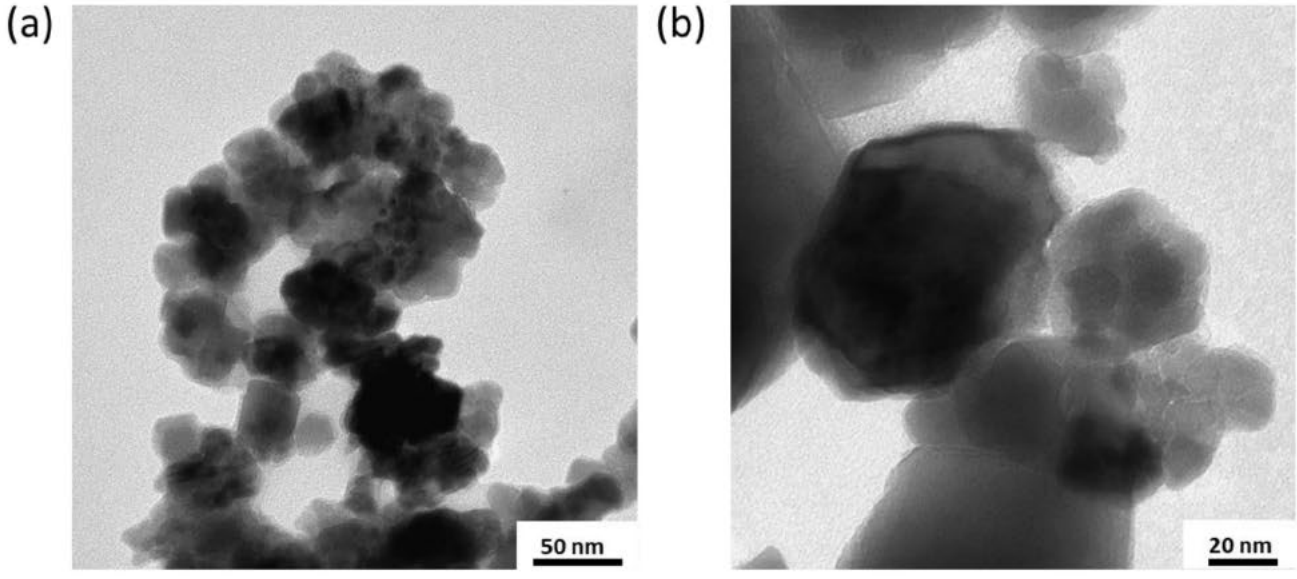


**Figure 11.** TEM micrograph images of $Cr_2O_3$ at magnifications of (a) × 100,000 and (b) × 200,000

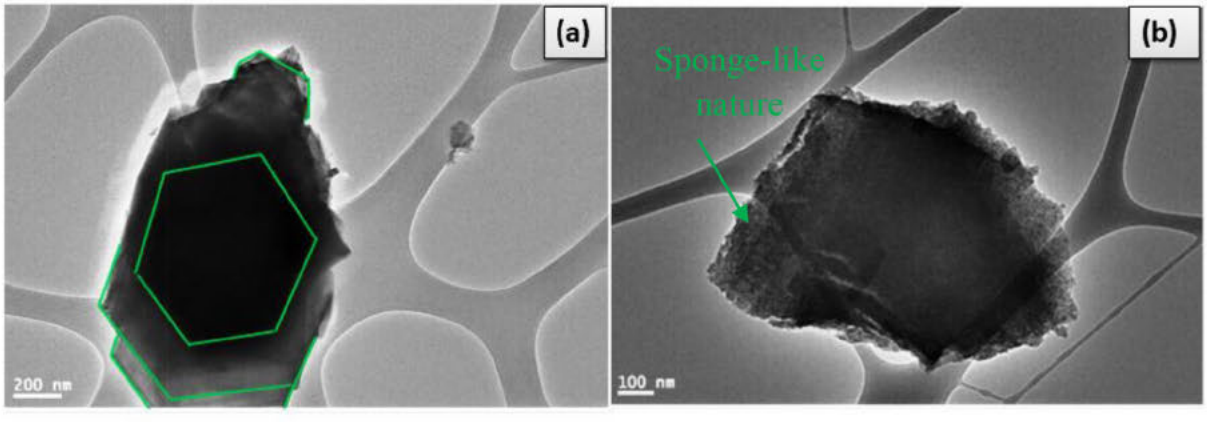


**Figure 12.** TEM micrograph images of $Cr_2S_3$ at magnifications of (a) × 40,000 and (b) × 60,000

The listed Miller indices (*hkl*) in Table 2 are used to identify different planes of atoms. Our crystal system displays the rotational symmetry operations for each lattice point as: x; y; z; *y; x* *y; z*; and *x* þ *y; x; z*. Because the rotational symme-try mixes *x* and *y* coordinates and leaves z coordinate unchanged, the corresponding Miller indices h and k would mix, as can be seen from the numerator of the first term of the planner spacing formula:

$$\frac{1}{d_{hkl}^2} = \frac{4}{3}\left(\frac{h^2 + hk + k^2}{a^2}\right) + \frac{l^2}{c^2} \quad (1)$$

where $d_{hkl}$ = $\lambda$=2sin$\theta$ and $\lambda$ = 1.54056 $A^0$ is the wavelength of the X-ray from Cu target of $K_a$ radiation. The lattice parameters are given by: a = b = 18.5286 Å; c = 18.6362 Å; $\alpha$ = $\beta$ = 90° and $\gamma$ = 120° . The above formula indicates that Miller indices h and k lead to the same planner spacing $d_{hkl}$ when exchanging their values.

## 2.5. TGA

Figure 6 illustrates the thermogravimetric analysis of $(C_6H_{11}NH_3)_3[Cr(NCS)_6] \cdot 3/2H_2O$, where the effect of temperature by heating on the sample weight was investigated under two different atmospheres: air (blue line) and helium gas (red line). The thermolysis was found to be stepwise (5-step thermal decomposition), irrespective of the atmosphere type.

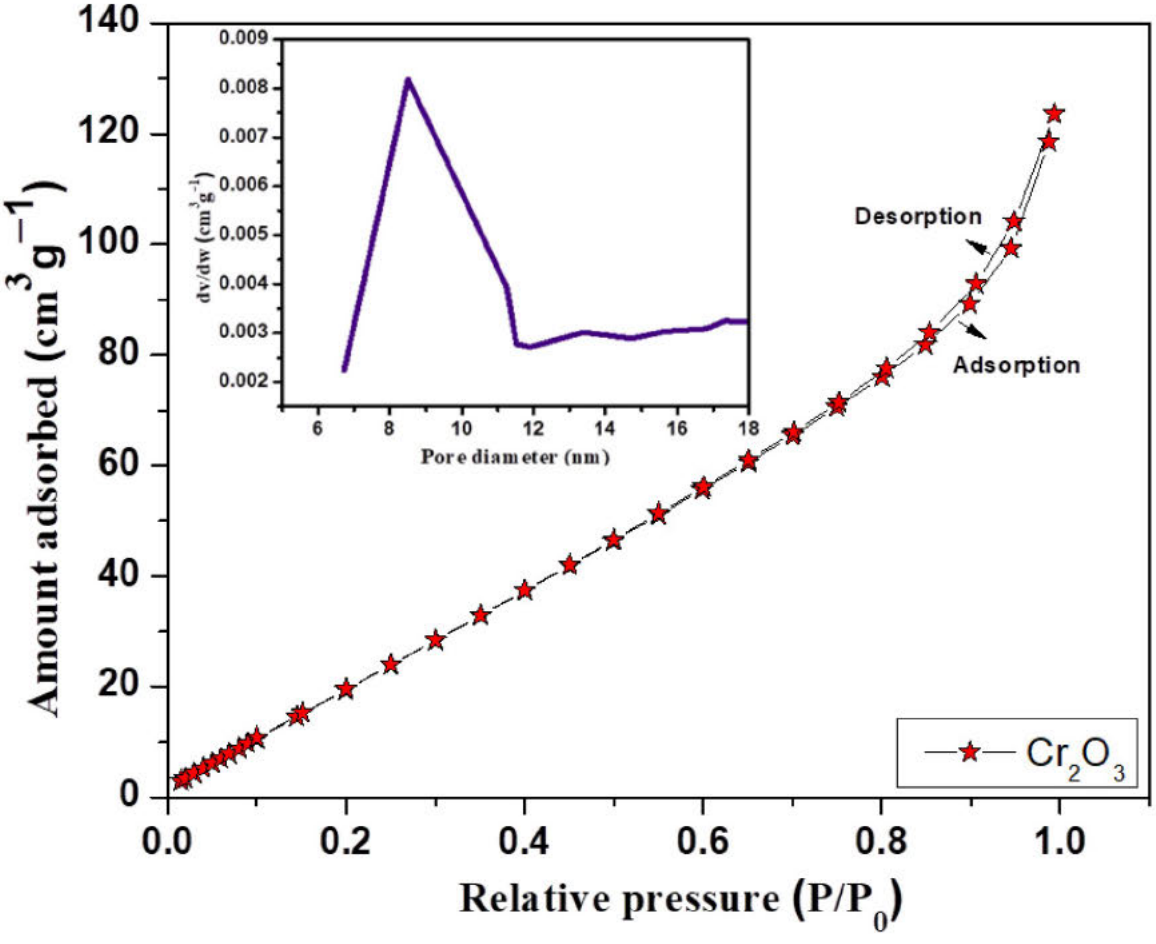


**Figure 13.** The nitrogen physisorption curves of $Cr_2O_3$ and BJH pore distribution (inset)

The complex started to decompose thermally under air atmosphere (Figure 6; blue line) upon heating from room temperature to lose ~ 3.71 % of its weight at temperature of ~150 C. This first step in weight lost corresponded to the loss of 1.5 water molecules, where the low temperature of losing water indicated that they were not coordinated to the Cr(III) ion center, but rather were crystallization molecules, a result in agreement with elemental, FTIR, UV-visible, and X-ray single-crystal analyses. The eventually produced anhydrous form of the complex at this stage, $(C_6H_{11}NH_3)_3[Cr(NCS)_6]$, lost one of its counter cations, $(C_6H_{11}NH_3)^+$, and one of its isothiocyanate ligands, NCS , at ~ 242 C, in the second step of decomposition. With raising the temperature to ~ 373 C, a loss of the remaining two $(C_6H_{11}NH_3)^+$ and one NCS ligand was observed in the third step of decomposition. The fourth step corre-sponded to the loss of one NCS ligand at ~ 396 C. The final step of decomposition linked to the loss of the remained three NCS ligands and the formation of chromia, $Cr_2O_3$, at ~ 576 C. The formation of $Cr_2O_3$ was assessed by calculating the remaining percentage weight (cal. 10.43 %; exp. ~ 10.25 %); and was corroborated by the PXRD analysis (Figure 7a).

On the other hand, the thermolysis of the complex under helium atmosphere was slower with enhanced thermal stability than what was observed under air atmosphere. The first step corresponded to the loss of the 1.5 water molecules of crystallization at ~ 168 C to result in the formation of the anhydrous form of the complex, which lost subsequently one $(C_6H_{11}NH_3)^+$ and one (NCS ) ligand at ~ 249 C, in the second step. The loss of the remaining two $(C_6H_{11}NH_3)^+$ could take place in the third step at ~ 338 C. The fourth step was due to the loss of four (NCS ) ligands and nitrogen atom ~ 600 C. The fifth step was due to the loss of carbon and the obtainment of $Cr_2S_3$ at ~ 700 C. The formation of $Cr_2S_3$ was corroborated by PXRD (Figure 7b). The formation of $Cr_2S_3$ was also deduced from thermolysis of piperidinium hexaisothiocyanatochromate (III), $(C_5H_{12}N)_3[Cr(NCS)_6]$, under dry nitrogen at 700 C.[57]

### 2.6. PXRD of thermal decomposition products of $(C_6H_{11}NH_3)_3[Cr(NCS)_6] \cdot 3/2H_2O$

Figure 7 (a) shows the PXRD pattern of the thermal decomposition of $(C_6H_{11}NH_3)_3[Cr(NCS)_6] \cdot 3/2H_2O$ at 600 C under air atmosphere. It revealed somewhat sharp, symmetrical basal

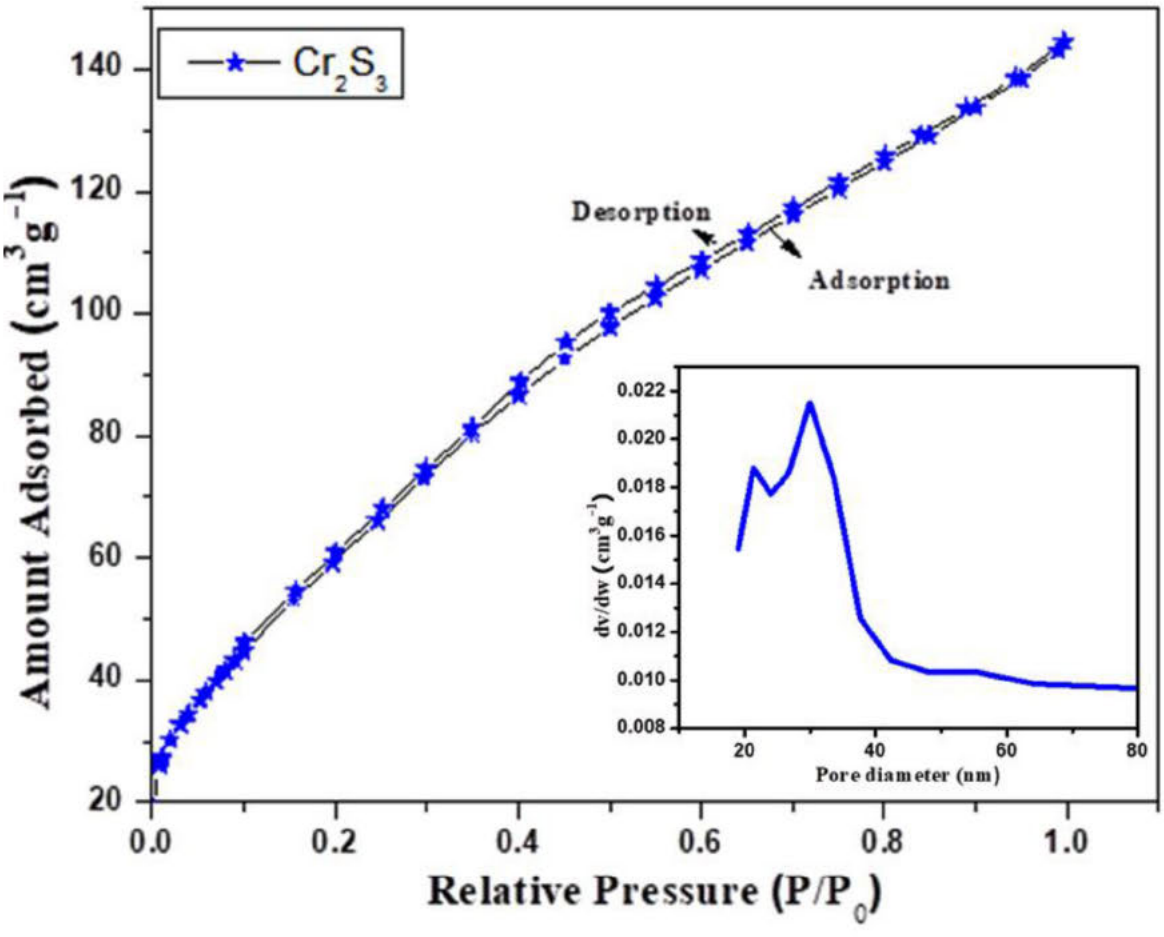


**Figure 14.** The nitrogen physisorption curves of $Cr_2S_3$ and BJH pore distribution (inset)

peaks at 2θ of 24.3, 33.4, 36.01, 38.6, 41.3, 43.3, 50.03, 54.6, 58.01, 63.19, 64.87, 72.59, 76.70, 79.94, 84.07, 86.35, 89.94, and 95.09 . These peaks were indexed to the characteristic peaks with Miller indices: (012), (104), (110), (006), (113), (202), (024),(116), (122), (214), (300), (101), (220), (306), (021), (134), (226), and (2110), respectively, of trigonal *eskolaite* phase of porous crystals of $Cr_2O_3$ (JCPDS 84-1616).[65]

Figure 7 (b) shows the PXRD pattern of $Cr_2S_3$, the thermal decomposition product of $(C_6H_{11}NH_3)_3[Cr(NCS)_6] \cdot 3/2H_2O$ at 730 C under helium atmosphere, having reflections at 2θ of 31.50, 38.78, 44.52, 45.27, 53.30, 56.32, 71.80, and 75.18 (PDF:10-0340). These characteristic peaks were indexed to:(112), (201), (203), (212), (205), (027), (008), and (224), respectively, for the trigonal phase.[72] In addition, the rhombo-hedral phase was detected with peaks at 2 theta 30, 34, and 58 assigned to the (110), (113), and (303) planes, respectively.[92]

Scherrer's equation was applied to calculate the crystallite size.[93]

$$D = \frac{0.90\lambda}{\beta \cos\theta} \quad (2)$$

Where the symbols:, θ, and β stand for the 1.5406 A Cu $K_\alpha$ line, Braggs' XRD diffraction angle, and the full width at half maximum (FWHM) in radians. The crystallite sizes were 52.62 and 39.16 nm for $Cr_2O_3$ and $Cr_2S_3$, respectively. On the other hand, the lattice parameters $a = b$ and $c$ were calculated by using the formula

$$\frac{1}{d^2} = \frac{4}{3}\left[\frac{h^2 + hk + k^2}{a^2}\right] + \frac{l^2}{c^2} \quad (3)$$

The values for $Cr_2O_3$ were a = b = 4.940 and c = 13.590 Å, in agreement with values reported in literature,[94] while for $Cr_2S_3$, the values were $a = b = 6.17$ and $c = 11.520$ Å, and the obtained data were greatly similar to previously reported data.[72]

In accordance with the Williamson-Hall method,[95] strain (ε) and crystallite size (D) have substantial contribution to the diffraction lines broadening (equation 3) where they are only

considered to reflect the peak width due to their to 2θ.[96,97] In the uniform deformation model *UDM* (equation 4) of William-son–Hall approach, it is assumed that crystals are isotropic[98] and subsequently their properties are independent of the crystallographic direction along which the measurement is performed.

$$b_{hkl}\cos\theta_{hkl} = \frac{k\lambda}{D} + 4\varepsilon\sin\theta_{hkl} \quad (4)$$

A plot of $b_{hkl}\cos\theta_{hkl}$ versus $4\sin\theta_{hkl}$ (θ corresponds to the (012), (104), (110), (024), (116), (122) and (214) planes of $Cr_2O_3$ and (112), (203), (212), (205) and (224) planes of $Cr_2S_3$ (Figure 8) is a linear graph,[92] where the crystallite size (*D**) and micro-strain (ε) can be respectively obtained from the intercept and slope (Figure 8). The crystallite sizes were 40.8 nm for $Cr_2O_3$ and 46.2 nm for $Cr_2S_3$ with an increased strain (ε) for the smaller size $Cr_2O_3$ nanoparticles (0.0006 and 0.0007 for $Cr_2S_3$ and $Cr_2O_3$, respectively). The average crystallite sizes estimated by using Scherrer's and W H methods exhibited disparity that could be ascribed to variation in particle size distribution averaging by using more peaks.[95]

### 2.7. SEM morphology investigation for $Cr_2O_3$

The scanning electron micrograph images of $Cr_2O_3$, prepared by the thermal decomposition at 600 C, are presented at two magnifications of × 5,000 (Figure 9a) and × 50,000 (Figure 9b). Agglomeration was observed for the $Cr_2O_3$ particles which demonstrated irregular polyhedron shapes (Figure 9).[62,67,68] This outcome was made possible due to the transportation of chromium oxide from smaller sized particles to ever increasingly larger sizes during the gas phase.[99] It is also well stablished that aggregation readily takes place in nanocrystals to decrease the high surface energy, leading to growth of clusters.[100] The qualitative surface elemental analysis by EDX (Figure S2 (A) of supplementary information) confirmed the presence of chromium and oxygen contents, while the quantitative analysis resulted in a very similar weight/weight percentage of each element to that of $Cr_2O_3$ bulk (Cr: cal. 68.42 %, exp. 68.90 %; O: cal. 31.58 %, exp. 31.10 %).

### 2.8. SEM morphology investigation for $Cr_2S_3$

The SEM images of $Cr_2S_3$, synthesized by thermal decomposition at 730 C, are shown at two magnifications of × 10,000 (Figure 10a) and × 35,000 (Figure 10b). The $Cr_2S_3$ particles were found to be arranged in irregular hexagonal packed layers with varied thickness and orientation for each hexagonal pack. The formation of these hexagonal packed layers could be due to the chemical vapor deposition of $Cr_2S_3$.[101,102] The presence of chromium and sulfur content was confirmed by the qualitative surface elemental analysis of EDX (Figure S1 (B) of supplementary information). Oxygen was also detected on the surface of $Cr_2S_3$, where the O had a weight/weight percentage of 6.32. The presence of oxygen is due to the tendency of metal sulfide to oxidation.[103]

The quantitative analysis showed weight/weight percentage of Cr (57.61 %) and of S (36.08), which were relatively close to those of $Cr_2S_3$ bulk (Cr: 51.95 %; S: 48.05 %). On the other hand, carbon was detected on the surface. Carbon might be either from some amorphous carbon present on the surface after calcination under helium or from the carbon tape used for sticking the sample on the holder.

### 2.9. TEM micrographs of $Cr_2O_3$ and $Cr_2S_3$

Figure 11 presents the TEM micrographs of $Cr_2O_3$ particles at two magnifications of × 100,000 (Figure 11a) and × 200,000 (Figure 11b). A conglomerate of $Cr_2O_3$ particles was observed with irregular shapes having multi faces, which agreed with the SEM results.

On the other hand, irregular hexagonal packed layers of $Cr_2S_3$ particles were also observed in the TEM micrograph images at magnifications of × 40,000 (Figure 12a) and × 60,000 (Figure 12b), which were consistent with those results obtained by SEM. Figure 12b shows the porous nature of $Cr_2S_3$, observed as sponge-like, a feature confirmed by the nitrogen physisorption measurements.

### 2.10. Adsorption of Nitrogen

Figures 13 and 14 depict the adsorption-desorption curves of nitrogen physisorption of $Cr_2O_3$ and $Cr_2S_3$, respectively. Type IV adsorption isotherms for mesoporous material were obtained for both chromium oxide and chromium sulfide, as per the IUPAC classification.[104] The amount of adsorbed nitrogen increased with relative pressure ($P/P_0$), where the adsorbed amount at specific pressure for $Cr_2S_3$ was much higher than that of $Cr_2O_3$. This observation was reflected by the higher specific surface area of $Cr_2S_3$ of 241.2 $m^2 g^{-1}$ with a t-plot external surface area of 331.9 $m^2 g^{-1}$ than that of $Cr_2O_3$ of 131.7 $m^2 g^{-1}$ with a t-plot external surface area value of 198.7 $m^2 g^{-1}$. In addition, the higher surface area of $Cr_2S_3$ was supported by the higher pore volume of 0.24 $cm^3 g^{-1}$ with a pore width of ~ 20 Å than that of $Cr_2O_3$ of 0.18 $cm^3 g^{-1}$ with a pore width of ~ 40 Å, as inferred from Barrett, Joyner, and Halenda (BJH) pore size distribution adsorption curves for $Cr_2O_3$ (Figure 13 inset) and for $Cr_2S_3$ (Figure 14 inset). The BJH pore size distributions of both of $Cr_2O_3$ and $Cr_2S_3$ were greater than 2.0 nm and less than 50 nm, i. e. were within the range of mesoporous according to IUPAC classification of porous materials.[104] The BJH pore size distribution of $Cr_2O_3$ was in the range of 7–12 nm, which was narrower than that of $Cr_2S_3$, which in the range of 20–40 nm. Furthermore, the pore size of $Cr_2O_3$ was much smaller than that of $Cr_2S_3$, as it could be concluded from the BJH pore size distribution. The formation of mesopores could be attributed to the action of cyclo-hexylammonium as a soft organic template.[20,105] Furthermore, the synthesis of stable mesoporous material is preferred at high temperature.[62] The BET surface area of the synthesized mesoporous $Cr_2O_3$ greatly exceeds the reported surface areas for $Cr_2O_3$ of 37.9 $m^2 g^{-1}$,[106] 23 $m^2 g^{-1}$,[67] 27 $m^2 g^{-1}$,[107] 81.05 $m^2 g^{-1}$,[108] and 21.14 $m^2 g^{-1}$;[109] and the BET surface area

of the obtained mesoporous $Cr_2S_3$ surpasses the reported surface area of 9 $m^2 g^{-1}$ for $Cr_2S_3$,[72] making mesoporous $Cr_2O_3$ and $Cr_2S_3$ potential candidates for adsorption and catalysis applications.

## 3. Conclusion

We prepared a novel organic-inorganic hybrid salt of cyclohexylammonium hexaisothiocyanatochromate(III) sesquihydrate via simple, economic approach based on metathesis and ligand addition. The validation for the formation of this desired compound came from elemental microanalysis, spectroscopic, and X-ray single crystal characterizations. The thermal decomposition of the material proved its utility as a single-source precursor for the production of mesoporous either $Cr_2O_3$ or $Cr_2S_3$, under air or inert atmosphere, with high specific surface area and micrometer size particles, though a self-templating mechanism by cyclohexylammoniun and high temperature for obtaining these two products. Both of $Cr_2O_3$ and $Cr_2S_3$ were nanocrystalline, as proven by their PXRD and the estimation of their average crystallite sizes by using Scherrer's and W H methods. Moreover, $Cr_2O_3$ showed polyhedron particles, while $Cr_2S_3$ had irregular hexagonal packed layers. All these textural and morphological properties make both of $Cr_2O_3$ and $Cr_2S_3$ suitable for many applications in catalysis, batteries, and sensing.

## X-ray crystallography

Deposition numbers 2043686 contains the supplementary crystallographic data for this paper. These data are provided free of charge by the joint Cambridge Crystallographic Data Centre and Fachinformationszentrum Karlsruhe Access Structures service www.ccdc.cam.ac.uk/structures.

## Supporting Information Summary

Detailed experimental of synthesis procedures and characterization methods are given in the SI. Tables for the crystals structures and labeled FTIR bands of cyclohexylammonium hexaisothiocyanatochromate(III) as well as the EDX spectra of $Cr_2O_3$ and $Cr_2S_3$ are provided in the SI.


## *Acknowledgements*

*We are grateful to King Abdulaziz City for Science and Technology (KACST), Saudi Arabia, for funding this work through project No. 20-0180.*


## *Conflict of Interest*

The authors declare no conflict of interest.


[1] H A Groenendijk, H W J Blöte, A J Van Duyneveldt, R M Gaura, C P Landee, R D Willett, *Physica* **1981**, *106B*, 47–58
[2] T Lis, L B Jerzykiewicz, *Acta Crystallogr.* **1995**, *C51*, 1001–1005
[3] K C K Swamy, M A Said, *Acta Crystallogr.* **2001**, *C5*, 7491–492
[4] S -S Yun, H -S Moon, C -H Kim, S -G Lee, *Coord. Chem.* **2004**, *57*, 321–327
[5] M Chellamuthu, S Kolandaivelu, S Krishnan, S Kandasamy, *Acta Crystallogr.* **2005**, *E61*, o3605–o3607
[6] T Kolev, B Koleva, R W Seidel, M Spiteller, W S Sheldrick, *Acta Crystallogr.* **2007**, *E63*, o4852
[7] D G Billing, A Lemmerer, *CrystEngComm* **2007**, *9*, 236–244
[8] D G Billing, A Lemmerer, *CrystEngComm* **2009**, *11*, 1549–1562
[9] A Lemmerer, *Cryst. Growth Des.* **2011**, *11*, 583–593
[10] X Wei, J Li, H Yin, *Acta Crystallogr.* **2011**, *E67*, o319
[11] M Sarr, C Merkens, A Diasse-Sarr, L Diop, U Englert, *Acta Crystallogr.* **2014**, *E70*, m220–m221
[12] A A Bagabas, M F A Aboud, A M Shemsi, E S Addurihem, Z A Al-Othman, C S C Kumar, H -K Fun, *Acta Crystallogr.* **2014**, *E70*, o253–o254
[13] W -Q Liao, H -Y Ye, D -W Fu, P -F Li, L -Z Chen, Y Zhang, *Inorg. Chem.* **2014**, *53*, 11146–11151
[14] A A Bagabas, S B Alhoshan, H A Ghabbour, C S Chidan Kumar, H -K Fun, *Acta Crystallogr.* **2015**, *E7*, o62–o63
[15] P Sathya, M Anantharaja, N Elavarasu, R Gopalakrishnan, *Bull. Mater. Sci.* **2015**, *38*, 1291–1299
[16] A Yangui, D Garrot, J -S Lauret, A Lusson, G Bouchez, E Deleporte, S Pillet, E Bendeif, M Castro, S Triki, Y Abid, K Boukheddaden, *J. Phys. Chem.* **2015**, *C119*, 23638–23647
[17] W Zhao, Y Jin, W Zhang, *Sci. China Chem.* **2016**, *59*, 114–121
[18] A Yangui, S Pillet, A Lusson, E Bendeif, S Triki, Y Abid, K Boukheddaden, *J. Alloys Compd.* **2017**, *699*, 1122–1133
[19] A Yangui, S Pillet, E Bendeif, A Lusson, S Triki, Y Abid, K Boukheddaden, *ACS Photonics* **2018**, *5*, 1599–1611
[20] A A Bagabas, M Alsawalha, M Sohail, S Alhoshan, R Arasheed, *Heliyon* **2019**, *5*, e01139
[21] M Kabesova, J Gazo, *Chem. Zvesti* **1980**, *34*, 800–841
[22] J E House Jr , G L Jepsen, *J. Inorg. Nucl. Chem.* **1978**, *40*, 697
[23] V Alexander, J L Hoppe, M A Malati, *Polyhedron* **1982**, *1*, 191–193
[24] F Berezovsky, S Triki, J S Pala, J R G -Mascaros, C J G -Garcia, E Coronado, *Synth. Met.* **1999**, *102*, 1755–1756
[25] T G Cherkasova, K V Mezentsev, *Russ. J. Inorg. Chem.* **2002**, *28*, 477–482
[26] M Mas-Torrent, S S Turner, K Wurst, J Vidal-Gancedo, J Veciana, P Day, C Rovira, *Eur. J. Inorg. Chem.* **2003**, *4*, 720–725
[27] F Thétiot, F Bérézovsky, S Triki, J S Pala, C J Gómez-García, A A Hajem, S Bouguessa, J -M Fabre, *C. R. Chim.* **2003**, *6*, 291–300
[28] E V Cherkasova, A V Virovets, E V Peresypkina, T G Cherkasova, E S Tatarinova, *Russ. J. Inorg. Chem.* **2006**, *51*, 557–562
[29] D Savard, D B Leznoff, *Dalton Trans.* **2013**, *42*, 14982–14991
[30] A C Brooks, L Martin, P Day, W Clegg, R W Harrington, J D Wallis, *Polyhedron* **2015**, *102*, 75–81
[31] J Kay, J W Moore, M D Glick, *Inorg. Chem.* **1972**, *11*, 2818–2826
[32] G Wrzeszcz, L Dobrzan'ska, A Wojtczak, A Grodzicki, *J. Chem. Soc. Dalton Trans.* **2002**, 2862–2867
[33] E V Cherkasova, A V Virovets, E V Peresypkina, N V Podberezskaya, T G Cherkasova, *Inorg. Chem. Commun.* **2006**, *9*, 4–6
[34] E V Cherkasova, E V Peresypkina, A V Virovets, N V Podberezskaya, T G Cherkasova, *Acta Crystallogr.* **2007**, *C63*, m195–m198
[35] E V Cherkasova, E V Peresypkina, A V Virovets, N V Podberezskaya, T G Cherkasova, *Russ. J. Inorg. Chem.* **2008**, *53*, 772–775
[36] E V Cherkasova, E V Peresypkina, A V Virovets, E S Tatarinova, T G Cherkasova, *Russ. J. Inorg. Chem.* **2008**, *53*, 1115–1120
[37] E V Cherkasova, A V Virovets, E V Peresypkina, T G Cherkasova, Yu R Giniyatullina, P G Chkov, **2009**, *54*, 370–376
[38] E S Tatarinova, *Russ. J. Inorg. Chem.* **2009**, *54*, 1625–1629
[39] A V Virovets, E V Peresypkina, E V Cherkasova, T G Cherkasova, N V Podberezskaya, *J. Struct. Chem.* **2009**, *50*, 137–148
[40] Yu R Giniyatullina, E V Peresypkina, A V Virovets, T G Cherkasova, E S Tatarinova, *Russ. J. Inorg. Chem.* **2012**, *57*, 811–814

[41] E V Cherkasova, E V Peresypkina, A V Virovets, T G Cherkasova, *Russ. J. Inorg. Chem.* **2013**, *58*, 1040–1046
[42] T G Cherkasova, E V Cherkasova, *Key Eng. Mater.* **2015**, *67*, 09–14
[43] E V Cherkasova, E V Peresypkina, A V Virovets, c, T G Cherkasova, *Russ. J. Inorg. Chem.* **2015**, *60*, 493–499
[44] A V Virovets, E V Cherkasova, E V Peresypkina, T G Cherkasova, *Z. Kristallogr.* **2015**, *230*, 551–558
[45] E V Cherkasova, E V Peresypkina, A V Virovets, T G Cherkasova, *Russ. J. Inorg. Chem.* **2016**, *61*, 174–179
[46] E V Cherkasova, E V Peresypkina, A V Virovets, T G Cherkasova, *Russ. J. Inorg. Chem.* **2016**, *61*, 447–450
[47] E V Cherkasova, N V Pervukhina, N V Kuratieva, I Yu Bagryanskaya, T G Cherkasova, *Russ. J. Inorg. Chem.* **2018**, *63*, 626–630
[48] E V Cherkasova, N V Pervukhina, N V Kuratieva, T G Cherkasova, *Russ. J. Inorg. Chem.* **2018**, *63*, 776–780
[49] E V Cherkasova, N V Pervukhina, N V Kuratieva, T G Cherkasova, *Russ. J. Inorg. Chem.* **2019**, *64*, 329–334
[50] R Belcher, S Liawruangrath, A Townshend, *Talanta* **1977**, *24*, 590–592
[51] M Q Al-Abachi, N A Shahbaz, S T Sulaiman, *Anal. Chim. Acta* **1981**, *125*, 215–218
[52] S A Rahim, T G Yakoob, M Q Al-Abachi, *Microchim. Acta* **1985**, *85*, 23–27
[53] M Q Al-Abachi, M S Al-Hafidh, S A Rahim, *Microchem. J.* **1988**, *37*, 110–113
[54] B Ptaszynski, E Skiba, *Thermochim. Acta* **1993**, *217*, 199–206
[55] B Ptaszynski, E Skiba, *Thermochim. Acta* **1993**, *223*, 93–100
[56] B Ptaszynski, E Skiba, *Thermochim. Acta* **2000**, *359*, 23–28
[57] J E House Jr, L A Marquardt, *Thermochim. Acta* **1989**, *145*, 265–269
[58] B Grzybowska, J Sloczynski, R Grabowski, K Wcislo, A Kozlowska, J Stoch, J Zielinski, *J. Catal.* **1998**, *178*, 687–700
[59] R Vijay, R Sundaresan, M P Maiya, S S Murthy, *J. Alloys Compd.* **2006**, *424*, 289–293
[60] W Yue, W Zhou, *Chem. Mater.* **2007**, *192*, 359–2363
[61] V Pintus, S Y Wei, M Schreiner, *Anal. Bioanal. Chem.* **2012**, *402*, 1567–1584
[62] P Xia, S Zuo, F Liu, C Qi, *Catal. Commun.* **2013**, *41*, 91–95
[63] X Zhang, G Ma, P Cheng, *Ceram. Int.* **2014**, *40*, 9693–9700
[64] Y Ramesh, P Thirumala Bai, B Hari Babu, N Lingaiah, K S Rama Rao, P S Sai Prasad, *Appl. Petrochem. Res.* **2014**, *4*, 247–252
[65] V Ibarra-Galvan, A Lopez-Valdivieso, C I Villavelazquez-Mendoza, J Santoyo-Salazar, S Song, *Part. Sci. Technol.* **2014**, *32*, 451–455
[66] Z Pei, X Zheng, Z Li, *J. Nanosci. Nanotechnol.* **2016**, *164*, 655–4671
[67] H Wang, Y Zhang, L Zhang, Y Guo, S Liu, F Gao, Y Han, G Feng, X Liang, L Ge, *RSC Adv.* **2016**, *6*, 84871–84881
[68] X Chen, X Chen, S Cai, J Chen, W Xu, H Jia, J Chen, *Chem. Eng.* **2018**, *334*, 768–779
[69] S Mikhail, V H J (San) de Beer, A Kodentsov, E M Van Oers, R A Van Santen, *J. Catal.* **1997**, *168*, 245–254
[70] S J Bao, C M Li, C X Guo, Y Qiao, *J. Power Sources* **2008**, *180*, 676–681
[71] P Lou, Y Tan, P Lu, Z Cui, X Guo, *J. Mater. Chem. A* **2016**, *41*, 6849–16855
[72] D Groeneveld, H Groß, A -L Hansen, T Dankwort, J Haasen, J Wollenstein, W Bensch, L Kienle, J Konig, *Adv. Eng. Mater.* **2019**, *21*, 1–7
[73] C Zhang, X Cai, Y Qian, H Jiang, L Zhou, B Li, L Lai, Z Shen, W Huang, *Adv. Sci.* **2018**, *5*, 1700375–1700386
[74] G M Sheldrick, *Acta Crystallogr.* **2015**, *A71*, 3–8
[75] M C Burla, R Caliandro, B Carrozzini, G L Cascarano, C Cuocci, C Giacovazzo, M Mallamo, A Mazzone, G Polidor, *J. Appl. Crystallogr.* **2015**, *48*, 306–309
[76] G M Sheldrick, *Acta Crystallogr.* **2008**, A *64*, 112–122
[77] O V Dolomanov, L J Bourhis, R J Gildea, J A K Howard, H Puschmann, *J. Appl. Crystallogr.* **2009**, *42*, 339–341
[78] G Brauer, *Handbook of Preparative Inorganic Chemistry*, Vol 2, Academic Press, New York, **1965**, 1374
[79] P Hoffmann, J A Lobo, *Microporous Mesoporous Mater.* **2007**, *106*, 122–128
[80] D Moon, J -H Choi, *Acta Crystallogr.* **2017**, *E73*, 755–758
[81] J P Devlin, *J. Chem. Phys.* **1989**, *90*, 1322–1329
[82] S P Ghosh, A Mishra, *J. Inorg. Nucl. Chem.* **1971**, *33*, 4199–4201
[83] A Mishra, P Singh, *J. Inorg. Nucl. Chem.* **1979**, *41*, 905–908
[84] L F Larkworthy, A J Roberts, B J Tucker, A Yavari, *J. Chem. Soc. Dalton Trans.* **1980**, 262–268
[85] W Linert, R F Jameson, V Gutmann, B Pouresmaeil, *J. Coord. Chem.* **1991**, *24*, 137–149
[86] R G Pearson, *J. Am. Chem. Soc.* **1963**, *85*, 3533–3539
[87] Z Kantarci, M Karabacak, M M Bülbül, *J. Incl. Phenom. Macro.* **2001**, *40*, 317–321
[88] E Łukowiak, W Stręk, B Jezowska-Trzebiatowska, *Z. Naturforsch.* **1981**, *36a*, 996–998
[89] T A Khvorost, L Yu Beliaev, E Potalueva, A V Laptenkova, A A Selyutin, N A Bogachev, M Yu Skripkin, M N Ryazantsev, N V Tkachenko, A S Mereshchenko, *J. Phys. Chem. B* **2020**, *124*, 3724–3733
[90] U Periyayya, C -H Hong, *Mater. Charact.* **2009**, *60*, 1305–1310
[91] B H O'Connor, D Y Li, *B. A. Adv. X-ray Anal.* **2001**, *44*, 96–102
[92] P Lou, Y Tan, P Lu, Z Cui, X Guo, *J. Mater. Chem. A.* **2016**, *4*, 16849–16855
[93] F T L Muniz, M A R Miranda, C Morilla dos Santos, J M Sasak, *Acta Crystallogr.* **2016**, *A 72*, 385–390
[94] K Anandan, V Rajendran, *Mater. Sci. Semicond. Process.* **2014**, *19*, 136–144
[95] A Khorsand Zak, W H Abd Majid, M E Abrishami, R Yousefi, *Solid State Sci.* **2011**, *13*, 251–256
[96] T Pandiyarajan, B Karthikeyan, *J. Nanopart. Res.* **2012**, *14*, 1–9
[97] P Bindu, S Thomas, *J. Theor. Appl. Phys.* **2014**, *8*, 123–134
[98] T Ungár, *J. Mater. Sci.* **2007**, *42*, 1584–1593
[99] A Escardino, S Mestre, A Barba, V Beltran, A Blasco, *J. Am. Ceram. Soc.* **2000**, *83*, 29–32
[100] C Yeqing, K M Byung, C C Byung, J H Jeong, H K Yang, *J. Am. Ceram. Soc.* **2013**, *96*, 3596–3602
[101] I Nakada, M Kubota, *J. Cryst. Growth* **1978**, *43*, 711–718
[102] J Chu, Y Zhang, Y Wen, R Qiao, C Wu, P He, L Yin, R Cheng, F Wang, Z Wang, J Xiong, Y Li, J He, *Nano Lett.* **2019**, *19*, 2154–2161
[103] F Yang, C Wu, Z Li, *J. Cent. South Univ.* **2014**, *21*, 715–719
[104] J B Condon, *Surface area and porosity determinations by physisorption: measurements and theory*, Elsevier, Amsterdam, **2006**, 72
[105] A Alshammari, M Mokhtar, R Arasheed, A Asayegh, A Bagabas, *Top. Catal.* **2019**, *62* (7–11), 795–804
[106] P Xia, S Zuo, F Liu, C Qi, *Catal. Commun.* **2013**, *41*, 91–95
[107] H Wang, Y Zhang, L Zhang, Y Guo, S Liu, F Gao, Y Han, G Feng, X Liang, L Ge, *RSC Adv.* **2016**, *6*, 84871–84881
[108] M Cherian, M S Rao, W -T Yang, J -M Jehng, A M Hirt, G Deo, *Appl. Catal. A* **2002**, *233*, 21–33
[109] M Aghaie-Khafri, M H KakaeiLafdani, *Powder Technol.* **2012**, *222*, 152–159
[110] R F K Gunnewiek, C F Mendes, R H G A Kiminami, *Mater. Lett.* **2014**, *129*, 54–56